

RESEARCH ARTICLE

Anthropogenic activities dominated tropical forest carbon balance in two contrary ways over the Greater Mekong Subregion in the 21st century

Baozhang Chen^{1,2,3,4}  | Alphonse Kayiranga^{2,3} | Mengyu Ge¹ | Philippe Ciais⁵ | Huifang Zhang² | Andy Black⁶ | Xiangming Xiao⁷  | Wenping Yuan⁸ | Zhenzhong Zeng⁹  | Shilong Piao^{10,11,12} 

¹School of Remote Sensing and Geomatics Engineering, Nanjing University of Information Science and Technology, 210044, Nanjing, China

²State Key Laboratory of Resource and Environmental Information System, Institute of Geographic Sciences and Natural Resources Research, Chinese Academy of Sciences, 100101, Beijing, China

³University of Chinese Academy of Sciences, 100190, Beijing, China

⁴Jiangsu Center for Collaborative Innovation in Geographical Information Resource Development and Application, 210023, Nanjing, China

⁵Laboratoire des Sciences du Climat et de l'Environnement, CEA-CNRS-UVSQ, Université Paris-Saclay, 91191, Gif-sur-Yvette, France

⁶Faculty of Land and Food Systems, University of British Columbia, British Columbia, Vancouver, Canada

⁷Department of Microbiology and Plant Biology, Center for Earth Observation and Modeling, University of Oklahoma, Oklahoma, Norman, USA

⁸School of Atmospheric Sciences, Guangdong Province Key Laboratory for Climate Change and Natural Disaster Studies, Zhuhai Key Laboratory of Dynamics Urban Climate and Ecology, Sun Yat-sen University, 510245, Guangdong, Zhuhai, China

⁹State Environmental Protection Key Laboratory of Integrated Surface Water–Groundwater Pollution Control, School of Environmental Science and Engineering, Southern University of Science and Technology, Shenzhen, China

¹⁰Sino-French Institute for Earth System Science, College of Urban and Environmental Sciences, Peking University, 100871, Beijing, China

¹¹Key Laboratory of Alpine Ecology and Biodiversity, Institute of Tibetan Plateau Research, Chinese Academy of Sciences, 100085, Beijing, China

¹²Center for Excellence in Tibetan Plateau Earth Sciences, Chinese Academy of Sciences, 100085, Beijing, China

Correspondence

Baozhang Chen and Alphonse Kayiranga, State Key Laboratory of Resource and Environmental Information System, Institute of Geographic Sciences and Natural Resources Research, Chinese Academy of Sciences, Beijing 100101, China.

Email: baozhang.chen@igsrr.ac.cn and akayiranga2018@igsrr.ac.cn

Mengyu Ge, Faculty of Agriculture and Forest, University of Helsinki, Viikinkaari 1, Biocentre 1, Helsinki 00790, Finland.
Email: mengyu.ge@helsinki.fi

Funding information

National Natural Science Foundation of China, Grant/Award Number: 41771114; National Key R&D Program of China, Grant/Award Number: 2018YFA0606001; Innovation Project of LREIS, Grant/Award Number: KPI005

Abstract

The tropical forest carbon (C) balance threatened by extensive socio-economic development in the Greater Mekong Subregion (GMS) in Asia is a notable data gap and remains contentious. Here we generated a long-term spatially quantified assessment of changes in forests and C stocks from 1999 to 2019 at a spatial resolution of 30m, based on multiple streams of state-of-the-art high-resolution satellite imagery and in situ observations. Our results show that (i) about 0.54 million square kilometers (21.0% of the region) experienced forest cover transitions with a net increase in forest cover by 4.3% (0.11 million square kilometers, equivalent to 0.31 petagram of C [Pg C] stocks); (ii) forest losses mainly in Cambodia, Thailand, and in the south of Vietnam, were also counteracted by forest gains in China due mainly to afforestation; and (iii) at the national level during the study period an increase in both C stocks and C sequestration (net C gain of 0.087 Pg C) in China from new plantation, offset anthropogenic emissions (net C loss of 0.074 Pg C) mainly in Cambodia and Thailand from deforestation. Political, social, and economic factors significantly influenced forest

Baozhang Chen and Mengyu Ge contributed equally to this work.

cover change and C sequestration in the GMS, positively in China while negatively in other countries, especially in Cambodia and Thailand. These findings have implications on national strategies for climate change mitigation and adaptation in other hotspots of tropical forests.

KEYWORDS

anthropogenic carbon uptake/emissions, carbon sequestration, forest cover changes, the Greater Mekong Subregion, tropical forest

1 | INTRODUCTION

Tropical forests, as the largest terrestrial component of the global carbon (C) cycle (Bonan, 2008), store C of 247Pg C (Saatchi et al., 2011). Anthropogenic-influenced tropical forest cover transitions have numerous impacts on both biotic and abiotic systems, including biodiversity, terrestrial C storage, hydrology, and climate across local, regional, and global scales (Alkama & Cescatti, 2016; Baccini et al., 2017; Brienen et al., 2015; Erb et al., 2018; Foley et al., 2005; Qin et al., 2019, pp. 2000–2017). As an important tropical forest with large C stocks and biological richness, the Greater Mekong Subregion (GMS; Figure S1) is under considerable anthropogenic threat (Davis et al., 2015) and it is a priority area for conservation policies (Namkhan et al., 2021). Rapid socio-economic development (Leinenkugel et al., 2015), different land use policies (Davis et al., 2015; Hansen et al., 2020; Tong et al., 2020; Zeng, Estes, et al., 2018), and disturbances (Yin et al., 2020) across the GMS have resulted in substantial and rapid forest cover changes (deforestation, reforestation, and afforestation) over the last three decades (Davis et al., 2015; Pungkul et al., 2014; Tong et al., 2020).

Between 1990 and 2010, the GMS has recorded about $8.01 \times 10^4 \text{ km}^2$ of forest loss (4.2% of the total land), with an average decreasing rate of 0.4% per year (Costenbader et al., 2015). For instance, during the first decade of this century, Laos People's Democratic Republic (Laos) and Cambodia had annual forest loss rates of 0.5% and 1.3%, these which are nearly four and 10 times higher than the global average, respectively (Leinenkugel et al., 2015). During 1990–2015, GMS's forest cover decreased by about 5.1%, which was characterized by high forest loss in Myanmar and Cambodia with annual deforestation rates of $4.66 \times 10^3 \text{ km}^2 \text{ year}^{-1}$ (1.5%) and $2.19 \times 10^3 \text{ km}^2 \text{ year}^{-1}$ (2%) (Gritten et al., 2019; MacDicken, 2015), respectively. Similarly to other subtropical regions, the GMS has been experiencing fast tree-cover loss owing to cropland expansion on hill slopes (Davis et al., 2015; Feng et al., 2021; Zeng, Estes, et al., 2018). In contrast, since 2000, woody vegetation cover in southern China has greatly increased (Brandt et al., 2018; Tong et al., 2018, 2020) as the results of China's government policies to combat land degradation by afforesting open and short-vegetation lands (Tong et al., 2018, 2020).

Different studies indicated that the adequate forest management and modern forest harvesting practices are a major influential way to change biomass C stocks and control terrestrial CO_2

cycles (Baccini et al., 2017; Chu et al., 2019; Kwon & Larsen, 2013). Quantitative evaluation of forest cover change and the associated CO_2 storage change is critical for understanding the mechanisms behind the terrestrial CO_2 cycles (Chu et al., 2019; Hui et al., 2017; Kwon & Larsen, 2013). Several methods for estimating spatiotemporal patterns of forest cover change and related C stock and C sequestration dynamics have been implemented and evaluated by different studies (Baccini et al., 2017; Hui et al., 2017; Pungkul et al., 2014; Zeng, Estes, et al., 2018). The combination of modeling and remote sensing technologies has the potential for estimating forest cover change as well as monitoring forest C storage and sequestration dynamics at a wide coverage (Qin et al., 2019, pp. 2000–2017). Remote sensing is the most efficient way to monitor land use and land cover (LULC) change over large¹ areas (Hansen et al., 2013). More and more freely available high-quality remote sensing data collected by a suite of state-of-the-art space-borne sensors (e.g., Landsat, Sentinel-1 and -2, MODIS, VIIRS, etc.) have been leading to improvement of algorithms for quantifying LC maps and forest dynamics from local to global scales (Hansen et al., 2013; Pungkul et al., 2014; Qin et al., 2019, pp. 2000–2017; Tang et al., 2021). It was proved that combining high-resolution remote sensing datasets with machine learning algorithms on high-performance cloud computing platforms, such as Google Earth Engine (GEE), can provide more accurate LULC maps which is the profound of accurate quantification of forest cover change, associated C stocks, and understanding the processes of forest C sequestration dynamics (Bofana et al., 2020; Fortin et al., 2020; Kayiranga et al., 2016, 2018; Keenan et al., 2012; Tong et al., 2018; Zheng et al., 2017).

Many global satellite-based forest cover products and forest assessment products including the Food and Agriculture Organization-Forest Resources Assessment (FAO-FRA) reports, have been produced to indicate the state of forest change (i.e., total area, spatial distribution, and tree biodiversity) across country to global scales (Chen et al., 2020). However, several evaluation studies indicated that these global forest cover products are inconsistent and even contradictory in some regions (Gardner et al., 2009; Hansen & DeFries, 2004, pp. 1982–99; Zeng, Estes, et al., 2018). For example, according to Song et al (Song et al., 2018), the global tree cover increased by $2.2 \times 10^4 \text{ km}^2$ from 1982 to 2016, the gross forest loss and gain both increased, with gain higher than loss; Hansen and DeFries (2004, pp. 1982–99) reported that global forest loss by $2.3 \times 10^6 \text{ km}^2$ and gain by $0.8 \times 10^6 \text{ km}^2$ from 2000 to 2012; a forest

loss of $1.3 \times 10^6 \text{ km}^2$ during 1990–2015 was reported by FAO-FRA; and a decrease in the tropical forest of $1.95 \times 10^4 \text{ km}^2$ during 1990–2015 was reported by Keenan et al. (2015). Most of the available forest cover change datasets are not accurate enough and are under debate (Chen et al., 2020). Considering the presented inconsistency in the exiting forest cover products in the study region, it is needed and very important to produce a 20-year series of land cover products over this region with higher resolution (30-m) and higher accuracy. Time series analysis using these high-resolution LC data would be an efficient way of providing temporally consistent assessment of LULC change (Tang et al., 2021).

The objective of this study is to map and quantify annual forest cover changes and related C sequestration dynamics at a 30-m spatial resolution and to investigate the major forest cover transitions and their effects on C sequestration during the period 1999 to 2019. We derived annual maps of land cover, C stocks, and C sequestration at a 30-m resolution on the GEE platform mainly based on the Landsat 7 Enhanced Thematic Mapper plus (LT7 ETM+) and Landsat 8 Operational Land Imagery (LC8 OLI) imagery data and ancillary data. To further study the impact of different forest cover transitions on C uptake, we stratified forest management over the whole region into five different types (Table 1) and nine forest-related land cover trajectory types and LULC-based C pools (Tables S4 and S5). The classification was based on mapping the duration, magnitude, and direction of human-induced disturbances from annual forest probability time series data (during 1999–2019 and at a 30-m resolution; see Section 2 for more details).

2 | MATERIALS AND METHODS

The methodological procedures used in this study were consecutively classified into six categories and are comprehensively summarized in Figure S3. All the processing steps were performed on the GEE cloud computing platform (Moore & Hansen, 2011) and ArcGIS

software version 10.6 (Kayiranga et al., 2018). For links of GEE scripts used in this study, see Data Availability Statement section.

We collected reference data covering the full period (1999–2019) by visual interpretation of Landsat time series and high-resolution images using a tool developed on GEE (<https://xjtang.users.earthengine.app/view/sample-interpretation>). For each sample unit, the Landsat time series data were used to determine whether LULC change occurred. Combination of high-resolution Landsat images and images from Google earth were then used to determine the LULC types before and after the change.

2.1 | LULC classification methods and classifier descriptions

To perform the classification processes, the random forest (RF) classifier (algorithm) was used to classify the designated six major LC classes (see the section of Training and Validation Sample Selection in Supporting Information and Table S3). The RF classifier is an ensemble machine learning algorithm based on decision tree supervised classification method (Bofana et al., 2020; C. Liu et al., 2020). Based on a number of studies (Li et al., 2014; L. Liu et al., 2020; Nitze et al., 2012; Zheng et al., 2017), RF has the greater power and capabilities to process complex data with large dimensions (i.e., data noise and overfitting) and to provide the improved classification results and more reliable accuracy comparing with other classification algorithms (Bofana et al., 2020).

The RF specifically provides multiple decision trees based on randomly selected subsets of training samples and variables. Additionally, the RF classifier uses the Gini index (generalization of the binomial variance) to measure inequality (Bofana et al., 2020). The calibration of RF classifier requires only two parameters, which are (1) number of classification trees and (2) the number of prediction variables used in each node to make the tree grow (Bofana et al., 2020; C. Liu et al., 2020). In this study, RF parameters were

TABLE 1 The forest land use (major forest cover transitions) and their corresponding landscape coverage and contributions to C dynamics in the Greater Mekong Subregion during 1999–2019.^a

Types	Management and occurring probability	Forest cover		Mean C density in Mg C	Mean C stocks in Pg C	C sinks (+) or sources (-) in Tg C
		% (of the region)	$\times 10^4 \text{ km}^2$			
Intact forest	Permanent dense and protected forests	48.07 ± 17.3	122.5 ± 44.1	123.1 ± 38.3	3.3 ± 1.9	93.6 ± 12.5
Afforestation	Non-forest to forest (fast/abruptly)	11.04 ± 7.3	28.15 ± 18.6	34.0 ± 11.5	1.6 ± 1.1	18.4 ± 2.9
Natural loss	Forest to non-forest (slow/seasonally)	0.07 ± 0.01	0.18 ± 0.03	0.9 ± 2.7	0.1 ± 0.3	-18.5 ± 2.1
Deforestation	Forest to non-forest (fast/abruptly)	9.53 ± 1.1	24.35 ± 2.8	19.2 ± 10.2	1.3 ± 0.6	-15.2 ± 1.3
Degraded forest	Forest to non-forest (slow/gradually)	0.48 ± 0.4	1.22 ± 1.0	2.1 ± 1.0	0.8 ± 0.3	-0.74 ± 0.1

^aThe forest land use types were defined based on the major forest cover transitions described in Table S3, sustainability probability was structured based on possible trajectories and possibility of changes from forest to non-forest and non-forest to forest. Mean carbon (C) density and C stocks were aggregated for estimates using the Valuation of Ecosystem Services and Tradeoff model, while net C sink values were aggregated from the estimated C sequestration. The values with ± indicate standard deviations and the values in parentheses are the contribution percentages. A Petagram of C (Pg C) is also known as a Gigaton (Gt), equals to 10^{15} grams or 1 billion tons. 1 Teragram (Tg) = 1 million tons (Mt) = 10^{12} grams = 10^{-3} Pg C = 10^{-3} Gt C. 1 megagram (Mg) = 10^6 grams (g) = 1 ton C.

optimized as follows: number of trees=100, variables at each split (mtry)=6, and minimum size of terminal node=1. RF classifier function (*ee.Classifer.smileRandomForest*) was applied on the GEE platform (Figure S3; see Supporting Information GEE codes).

2.2 | Mapping forest cover probability and validation

Forest and non-forest pixels were extracted from the classified LC maps, where the non-forested pixels were reclassified as non-forest type while forest pixels were kept as forest type in new LC maps. In this study, at least a total number of 7720 validation sample points were acquired from FROM-GLC 10 ref. (Gong et al., 2019) and distributed over the two final classes namely forest and non-forest classes. Therefore, the forest and non-forest-related binary values were spatially used to establish the confusion matrix as a cross-tabulation to assess the mapping errors (commission and omission errors) by comparing the mapped and the ground observed class labels. The accuracy assessment metrics including producer's accuracy (PA) and user's accuracy (UA), kappa coefficient (K_C ; ranging: -1 and +1), and the overall accuracy (OA; in percentages) were evaluated to represent the commission-omission errors and the overall agreement between the mapped LC and ground truth (Thanh Noi & Kappas, 2018; Zheng et al., 2017). The values of K_C less than zero indicate no agreement between observed and predicted data, while the values close to 1 indicate excellent agreement (Bofana et al., 2020; Nitze et al., 2012; Thanh Noi & Kappas, 2018; Zheng et al., 2017). K_C was estimated using the following equation (Equation 1):

$$K_C = \frac{\sum_{i=1}^k x_{ii} - \sum_{i=1}^k (X_{i+} \times X_{+i})}{N^2 - \sum_{i=1}^k (X_{i+} \times X_{+i})}, \quad (1)$$

where k is number of rows and columns in the error matrix; N is the total number of observations; X_i represents observations in row i and column i ; X_{i+} stands for the marginal total of row i ; and X_{+i} indicates the marginal total of column i .

2.3 | Analysis of forest cover change and the degree of change

The annual forest cover change and the degree of changes were analyzed based on the distinguished forest and non-forest pixels using the two indices: K index and S index. K index is usually employed to calculate the LULC dynamic index as a percentile (%) of changes between the initial and final LULC maps at certain analysis period (T). The S index is usually employed to analyze the LULC dynamic (Huang et al., 2018; Lin et al., 2018, pp. 1992–2018). In this study, the indices K and S were applied to forest maps to analyze the trends and degree of changes of forest cover. The two indices were calculated using Equations (2 and 3):

$$K = \frac{F_{C_2} - F_{C_1}}{F_{C_1}} \times \frac{1}{T} \times 100\%, \quad (2)$$

$$S = \left(\sum_{ij}^n \left(\frac{\Delta A_{i \rightarrow j}}{A_i} \right) \right) \times \frac{1}{T} \times 100\%, \quad (3)$$

where F_{C_1} and F_{C_2} are the forest cover maps at the final and initial years, respectively, of a certain period; A_i is the area of forested land at the initial year of the period; $\Delta A_{i \rightarrow j}$ is the total area of forested land (i) converted into non-forest (j), and $\Delta A_{i \rightarrow j}$ is used to analyze the degree of forest loss while $\Delta A_{j \rightarrow i}$ is used to estimate the degree of forest gain; T represents the study time or the number of years considered for the index (Huang et al., 2018; Lin et al., 2018, pp. 1992–2018). In this study, the forest-K and S indices are estimated at the annual basis (annual change) and T is set to be 2 in each scenario.

2.4 | Analysis of major forest cover transition processes and related ecological classification

Major forest cover transitions are the processes of converting forested pixels to non-forest pixels and non-forest pixels being reforested or afforested (Leinenkugel et al., 2015; Qin et al., 2019, pp. 2000–2017; Yasmi et al., 2017). We developed an approach to identify the potential probability transitions that may generally affect forest cover pixels. This approach includes three steps: (1) to group LC maps as T1 (older) and T2 (newer); (2) to analyze the nine possible LC trajectory labels and assign them to specific LC transition probabilities; and (3) to designate and categorize the landscape change based on possible forest-related transition driving factors (Münch et al., 2019).

Therefore, high priority is given to the trajectories related to the potential forest loss and gain including forest encroachment, deforestation, afforestation/reforestation, and natural dynamics to account for encounter anthropogenic activities and natural climate-based effects (i.e., fire, drought, flooding, and erosion) that may have negatively effects on forest extent.

Table S4 shows the possible LC trajectory labels and transition probabilities (expected changes). The highlighted fields indicate the identified labels and transition possibilities that may affect forest cover; (↑) indicates increasing processes, and (↓) indicates decreasing processes. Landscape changes were categorized by gradual ecological change, abrupt change, and seasonal change. Moreover, to identify and compute the amount of forest loss and gain, pixels of unchanged forests consisting of persistent forests and protected forests were aggregated and named intact forest; the pixels of forest encroachment (forest converted into cropland), tree logging (deforestation), degradation and naturally forest loss trajectories were aggregated into deforestation or forest extraction and provided forest loss pixels; whereas all non-forest LC trajectories converted into forest provided forest gain pixels (i.e., afforestation, reforestation, and naturally forest regeneration).

2.5 | Estimates of forest-based C sequestration

The Integrated Valuation of Ecosystem Services and Tradeoffs (InVEST) C model was used to estimate forest-based C storage and

sequestration based on the four basic C pools (Figure S2) and forest cover pixels (Bierbower, 2015; Liang et al., 2017). To estimate and specifically separate the C storage and sequestration extent at forest and non-forest grid cells, the C values of each pool (C above, C below, C soil, and C dead) were aggregated over the forest and non-forest pixels (Table S5).

To train the InVEST C model and to calibrate the required inputs, the C pools (stated above) were first multiplied by 0.01 to convert their initial values from Mg C km⁻² to Mg C ha⁻¹ to match the metrics with the LC extent area metric (ha⁻¹) and a biophysical table was independently built based on forest and non-forest corresponding C pool pixels as shown in Table S5.

The total C storage C was given by the sum of C_{m,i,j} at a given grid cell (i, j) with LC type (m) and was estimated by the following equations (Equations 4 and 5):

$$C = \sum_{m=1}^n C_{m,i,j}, \quad (4)$$

$$C_{m,i,j} = A + Ca_{m,i,j} + Cb_{m,i,j} + Cs_{m,i,j} + Cd_{m,i,j}, \quad (5)$$

where A is the actual area of each forested or non-forested grid cell, Ca_{m,i,j}, Cs_{m,i,j}, Cb_{m,i,j} and Cd_{m,i,j} are the C stocks (in Mg C ha⁻¹) of aboveground biomass, belowground biomass soil organic C, and dead organic C at (i, j) with LC type (m). C sequestration S was therefore calculated using Equation (6):

$$S = C^{T2} - C^{T1}, \quad (6)$$

where C^{T2} and C^{T1} indicate the C storage values in years T1 and T2, respectively (Bierbower, 2015).

3 | RESULTS AND DISCUSSION

3.1 | Spatiotemporal forest cover dynamics

Annual LC maps at a 30-m resolution indicate that the total forest area increased from 1.42 × 10⁶ km² (55.0% of the region area) in 1999 to 1.53 × 10⁶ km² (59.3% of the region area) in 2019 (Figure S4). During the period 1999–2019, the forest-related LC trajectories were characterized as (Figure 1; Table S6; Figure S4): (i) there were 5.42 × 10⁵ km² (21.12% of the region area) experienced forest cover transitions (Figure 1a) and intact forest was mainly located in Laos PDR and Myanmar (Figure 1b); (ii) there was 0.47% forest change annually on average over the region area, with a decreasing trend during the period 1999–2009 at a rate of -1.74% year⁻¹ and an increasing trend during 2009–2019 at a rate of 2.21% year⁻¹ of the region area (Figure 1f,g; Figure S4A); (iii) cropland increased by 4.75% of the region area (Figure S4B) from encroachment in forest (Fe), land reclamation (Re), and increased cultivation land (Ic), where it mainly occurred in Thailand and Cambodia; and (iv) urban and settlement (Ue) increased about 0.03% of the region area. Analysis

of major forest cover transitions revealed that, of the GMS forest, there was approximately 11.04% afforested/reforested (Af), 9.53% deforested (transformed to agricultural land, i.e., forest encroachments-Fe) by human activities at forest boundaries, and only 0.07% forest loss due to natural disturbances (Table S6).

Figure 1 and Figure S5 show forest cover transition dynamics over the GMS at a country level during 1999–2019. A large forest gain (afforestation) mainly occurred in southern China (Yunnan and Guangxi provinces). Afforestation here did not include large-scale harvesting, but often included forestation of bare ground and short vegetation (grassland and cropland), especially continued forest expansion of croplands on hill slopes (a close-up is shown in Figure 1c). Forest cover increased substantially in Yunnan and Guangxi provinces of China, from 44.95% of the land in 1999 to 70.41% in 2019 with an average rate of increase of 80.22 km² year⁻¹ (1.27% year⁻¹ of the region; Figure S5K,L). The expansion of forested area and reduction of agriculture on marginal sloping lands was mainly due to the implementation of forestation policies since 2000, which includes government-funded efforts to combat land degradation and fight poverty (Brandt et al., 2018; Delang & Yuan, 2016; Tong et al., 2018, 2020).

In contrast, forest loss (deforestation) mainly occurred in Thailand (Figure 1d; Figure S5E), Cambodia (Figure 1e; Figure S5G), and South of Vietnam (Figure S5C). In Vietnam, deforestation was fast during the period 1999 to 2013 with an average forest loss rate of 0.23% year⁻¹ (7.87 km² year⁻¹) of the country's forest area (Figure S5C,D). In Cambodia, deforestation driven by large-scale land acquisitions (Davis et al., 2015) and other land use expansions (Feng et al., 2021; Grogan et al., 2019) has been accelerating since 2000. During the period 1999–2019, about 18% (0.93% year⁻¹ or 16.84 km² year⁻¹) of the country's forest area was lost through these land concessions (Figure S5G,H; see expanded view in Figure 1e), largely owing to acquired lands due to a surge in economic land concessions (Davis et al., 2015). Davis et al. reported that the annual rate of forest loss within concessions was between 29% and 105% higher than in comparable land areas outside concessions (Davis et al., 2015). Grogan et al. (2019) reported that 23.5 ± 1.8% of Cambodia's forest cover was cleared during the period 2001–2015. Other GMS countries showed a slight loss or nearly neutral change in forest area (Figure S5A,B,I,J). The total forest losses were offset by a large gain in forest area in China; as a result, the GMS has increased forest coverage by 1.92% since 1999 (Figure 1f; Figure S4A).

3.2 | Spatiotemporal distributions of forest C stocks and C sequestration

In this study, C sequestration was calculated from forest growth without considering the full life cycle of extracted wood. Changes in litter, coarse woody debris, and soil C were ignored as well. C sinks and sources of different forest land use types were aggregated from their corresponding C sequestration pixels over the period 1999–2019.

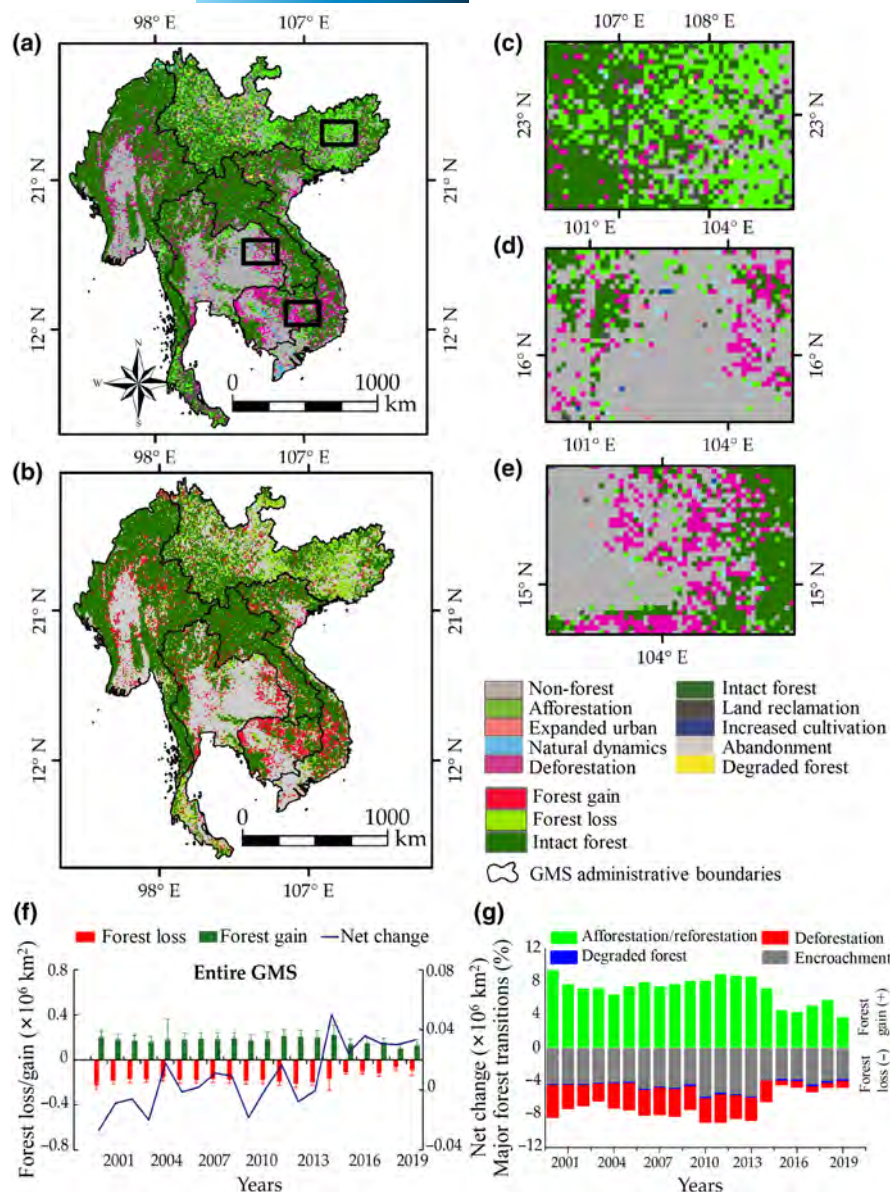
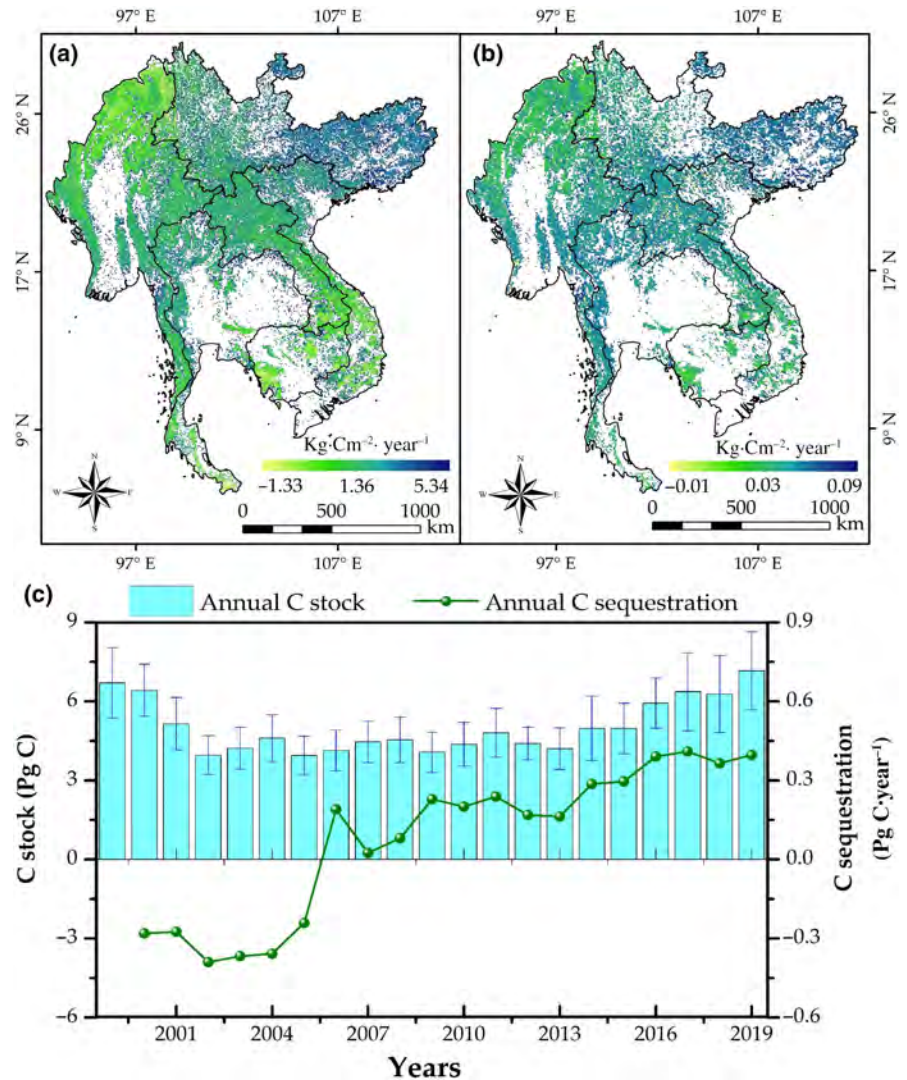


FIGURE 1 Spatial patterns and changes of forest cover transitions and net forest gain/loss in the Greater Mekong Subregion during 1999–2019. (a) Map of transitions of forests and other land cover. (b) Map of loss and gain of forests. (c) Expanded view of the upper black rectangle in (a), afforestation particularly common in northern Guangxi and Yunnan. (d) Expanded view of the middle black rectangle in (a) deforestation is particularly common in northwest Thailand. (e) Expanded view of the lower black rectangle in (a) deforestation which is particularly common in Cambodia is due to large-scale land acquisitions. (f) Annual loss, gain, and net change of forests, and the error bars indicate ± 1 standard deviation. (g) Aggregated major forest cover transitions contributed to forest loss and gain during 1999–2019. Map lines delineate study areas and do not necessarily depict accepted national boundaries.

Spatiotemporal distributions of C stocks and C sequestration in the entire GMS region and at a country level are shown in Figures 2 and 3 and Figure S6. The pixels with high values of both C stocks and C sequestration were in northeast Myanmar, Southern Cambodia, and South Vietnam (Figure 2a,b). Over the GMS, the total C stocks of 6.7 Pg C in 1999, decreased to 4.31 Pg C in 2006 and then increased to 7.36 Pg C in 2019 at a rate of 0.033 Pg C year⁻¹ (9.39% year⁻¹). Consequently, the major forest cover transition-induced C balance was inverted from a source before 2006 to a sink, and total C sequestration increased rapidly from 0.021 Pg C in 2007 to 0.41 Pg C in 2019 at the rate of 0.072 Pg C year⁻¹ (Figure 2c). Consistent with a case study in southern China,¹² the trends and inter-annual variability over the GMS region in C sequestration were expected to be controlled by the biogeochemical consequences of land use changes (Figure 2).

The total forest C stocks of the six countries during the period 1999–2019 varied from the lower values of 1.23 Pg C (Thailand) and 1.57 Pg C (Cambodia) to the highest values of 2.87 Pg C (Myanmar) in 1999 (Figure 3a). China was characterized by the largest C gain (1.75 Pg C) and the smallest C loss (0.15 Pg C), whereas Cambodia was characterized by the smallest C gain (0.38 Pg C) and the largest C loss (0.72 Pg C; Figure 3a). The forest C density for all the six countries increased during the study period with annual rates ranging from 0.12 ± 0.08 Mg C ha⁻¹ year⁻¹ (Cambodia) to 0.57 ± 0.12 Mg C ha⁻¹ year⁻¹ (China; Figure 3b). China, Myanmar, and Laos PDR showed higher increasing trends in C density owing to higher rates of increasing forest coverage in these countries (Figure 3b; Figure S6). Forest C sequestration decreased with a rate of 11.25 Mg C year⁻¹ in Cambodia and 3.22 Mg C year⁻¹ in Thailand while the other four countries increased with rates ranging from 17.55 to 35.55 Mg C year⁻¹ during 1999–2019 (Figure 3c).

FIGURE 2 Spatiotemporal changes in C stocks (a) and C sequestration (b) in the Greater Mekong Subregion (GMS) during 1999–2019. (a, b) Spatial distributions of mean annual changes in C stocks of forests and mean annual C sequestration, respectively, both are in $\text{kg Cm}^{-2} \text{year}^{-1}$ during the study period. (c) Total C stocks and annual C sequestration in the GMS. Map lines delineate study areas and do not necessarily depict accepted national boundaries.



3.3 | Impacts of forest cover change on C sequestration

Forest cover changes in this region have profound biophysical impacts on C dynamics. The association of the different LC types with C sequestration is shown in Figures 3 and 4 and the spatial distributions are shown in Figure 1a–e. Intact forests are permanent and protected forests with a dense tree cover and neutral disturbances (Table 1). Intact forests covered $1.24 \times 10^6 \text{ km}^2$ (48.07% of the region) and stored 41.42% of the total forest C stocks (3.28 Pg C) in the beginning of the study period (1999), and showed C stock gross gain of 0.95 Pg C and loss of 0.2 Pg C (Figure 3d), contributing to 3.2% of the region's forest C sequestration ($0.027 \text{ Pg C year}^{-1}$; Figure 3f) with a large increase in forest C density ($1.5 \text{ Mg C ha}^{-1} \text{ year}^{-1}$; Figure 3e) during the study period. On average of our study period, the intact forest sequestered $93.58 \text{ Mg C year}^{-1}$ accounting to 44.7% of the region's forest C sequestration (Table 1; Figure 3d). C sequestration by intact forests increased by $29.22 \text{ Mg C year}^{-1}$ ($3.2\% \text{ year}^{-1}$; Figure 3f) likely owing to CO_2 fertilization, global warming, and recovery from past disturbances.

Afforestation here includes all new forests (i.e., afforestation (afforested–reforested land and recovered forests), reforestation, and recovered forests) which is an area changed from non-forest to forest (Table 1). The afforestation land covered only 11.04% ($2.81 \times 10^5 \text{ km}^2$) of the region and stored 19.17% and 25.76% of the total forest C stocks (0.8 and 1.7 Pg C) at the beginning (1999) and at the end (2019) of the study period, respectively (Figure 3d), with a large forest C stock gain (1.68 Pg C) and an increase in forest C density (an average rate of $1.72 \text{ Mg C ha}^{-1} \text{ year}^{-1}$; Figure 3d,e). On average of the study period, afforestation stored 1.55 Pg C with forest C density of $33.96 \text{ Mg C ha}^{-1}$ and contributed to 26.02% of the total region's increase in forest C stocks. Afforestation sequestered $0.021 \text{ Pg C year}^{-1}$ and contributed to 27% of the GMS's forest C sequestration (Table 1; Figure 4). C sequestration by afforestation increased by $37.22 \text{ Mg C year}^{-1}$ ($3.8\% \text{ year}^{-1}$; Figure 3f) mainly owing to an increase in C density (Figure 3e).

Forest extraction was identified as three land use types (see Section 2 for their definitions) involving natural forest loss (NL), deforestation (Defo), and degraded forest (DF; Table 1). NL and DF, characterized by the gradual ecosystem landscape changes, were

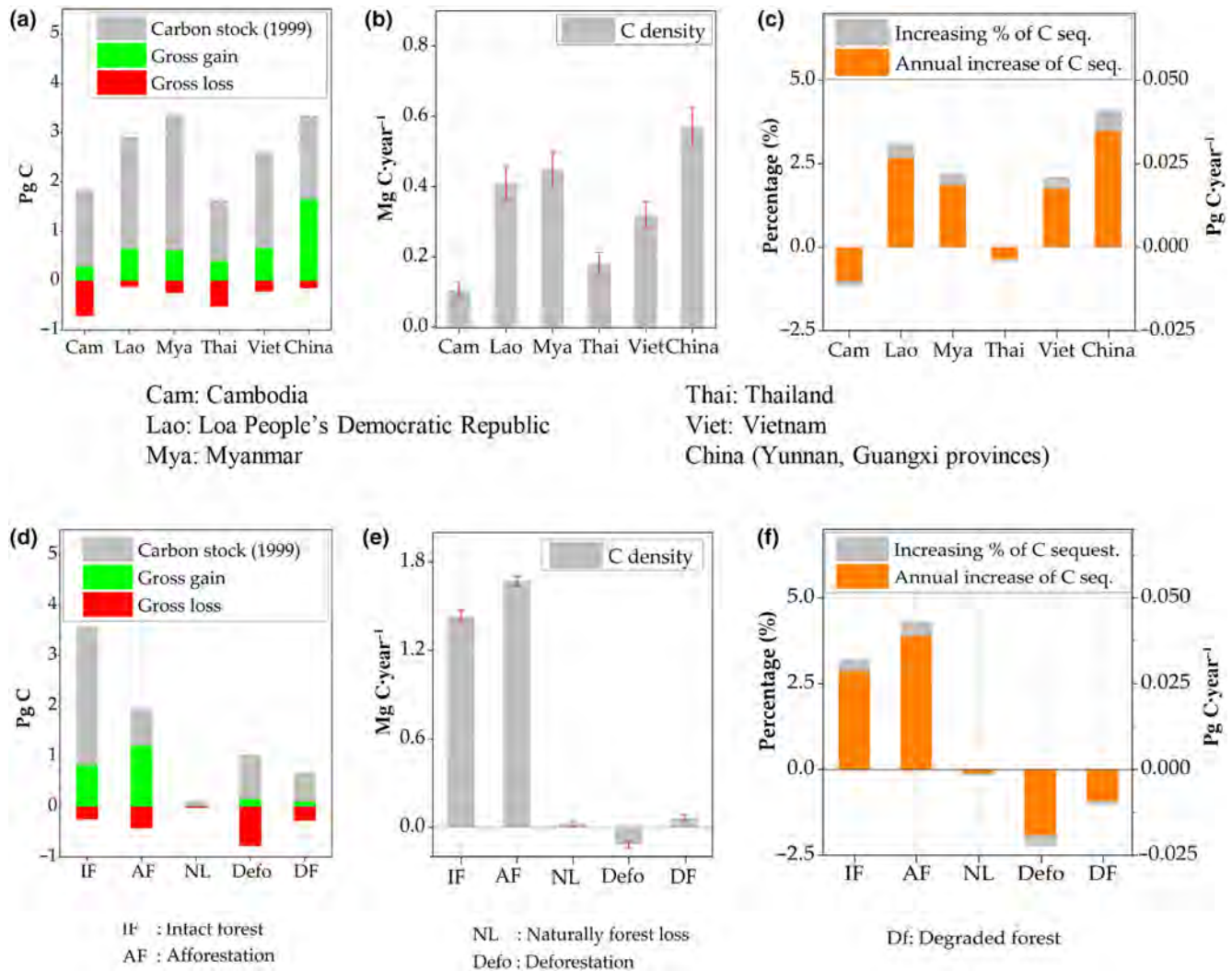


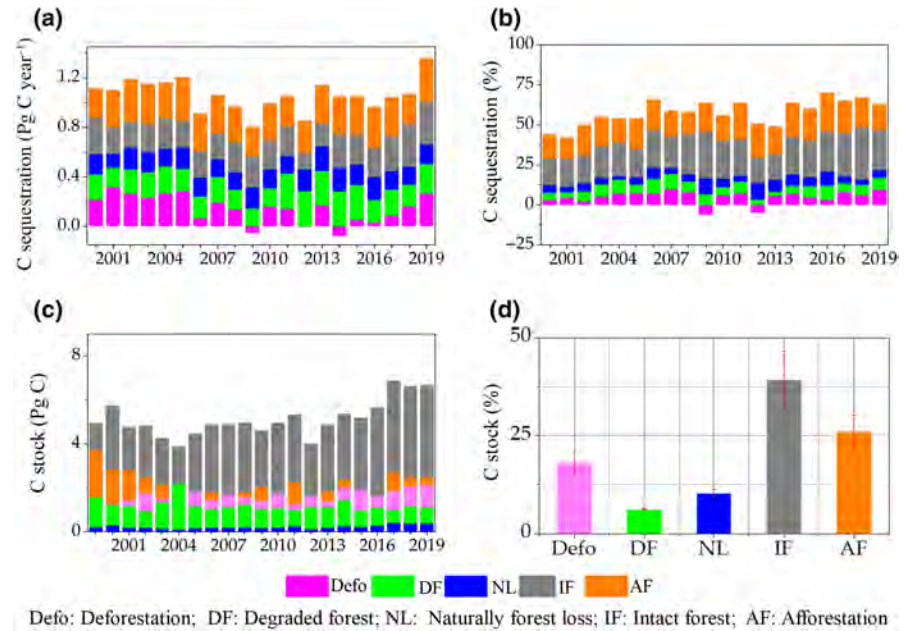
FIGURE 3 Dynamics of C stocks for different forest land use types in the Greater Mekong Subregion region and at country levels. (a) C stock in 1999, with consecutive gross gains and losses during the period 1999–2019. (b) Net changes in C density (1999–2019) and the error bars indicate ± 1 standard deviation. (c) Mean annual increasing rates of C sequestration in Pg C year^{-1} and increasing percentages (%) of its mean values during 1999–2019 for each country. (d), (e), and (f) are same as (a), (b), and (c), but for each forest land use type, respectively.

mainly caused by climate change and by anthropogenic activities at forest boundaries, including natural conversions of forests into marshlands, wetlands, and any other related wetlands (Table S4). Defo was a result of logging activities and other forest disturbances. The total forest extraction land covered 10.08% of the region ($2.61 \times 10^5 \text{ km}^2$) and had a net loss of 1.08 Pg C of forest C stocks and a decrease in C density with an average rate of 0.15 Mg Cha^{-1} per year during the period 1999–2019 (Figure 3d–f). C stocks of NL, Defo, and DF were 0.12, 0.88, and 0.67 Pg C in 1999 (Figure 3d), with a negative net balance (-0.05 , -0.71 , and $-0.18 \text{ Pg C year}^{-1}$), respectively, between 1999 and 2019 (Figure 3d). C sequestration of these three land use types with forest extraction decreased 1.2, 20.1, and $11.2 \text{ Mg C year}^{-1}$ and a contribution of 0.17%, 2.22%, and 1.02% to the regional C sequestration, respectively, whereas Defo and DF areas acted as a C source (Figure 3f) from 1999 to 2019.

3.4 | Accuracy assessment and data intercomparison

We evaluated the accuracy of our land cover results by comparing our results with other available multi-temporal land cover products (VCF, ESA-CCI, and MCD12 C1) at pixel levels. The intercomparison indicates that an overall agreement was found during 2010–2016 and high inconsistencies were found during 2001–2007 among all the available datasets (Figure S7A). A net forest gain of the GMS over this century was reported by MCD12, VCF, FRA and this study, whereas ESA-CCI is the only dataset showing an overall net forest loss of approximately $0.0115 \text{ Mha year}^{-1}$ (Figure S7B). Our estimated forest cover maps agree with observed forest maps (FROM-GLC 10, GSPECLib, and GEE) well with an overall agreement percentage of 87.85% and a kappa coefficient value of 0.86 (Table S7).

FIGURE 4 Effects of land use change on C dynamics. (a) Annual contributions of each forest land use type on C sequestration in Pg C year⁻¹. (b) Annual contributions of each forest land use type on C sequestration in percentage of the Greater Mekong Subregion region in %. (c) Annual C stocks of each major forest land use type in Pg C. (d) Comparative contribution of each forest land use type to the total C stocks of the region in %.



4 | CONCLUSION AND IMPLICATIONS

In the past two decades, the GMS has been characterized by extensive forest cover transitions owing to human activities and climate change. About $1.1 \times 10^5 \text{ km}^2$ of forest (4.31% of the region) transitioned to agricultural land through encroachment into forests, climate-related disasters, and other anthropogenic disturbances. The transitions mainly occurred in Cambodia, Thailand, and in the south of Vietnam with an overall regional forest loss of $2.5 \times 10^5 \text{ km}^2$ (9.80% of the GMS region in 1999) during 1999–2019 (Table 1; Table S5). This regional gross forest loss was compensated by afforestation and other transitions from traditional agriculture toward managed forests mainly as a result of a policy of the production of wood products established in the subtropical and mountainous landscapes in southern China (Yunnan and Guangxi provinces; Tong et al., 2020). We found that there were $2.8 \times 10^5 \text{ km}^2$ of afforested/reforested and recovered forests (10.98% of the GMS region area).

In the dynamic environments of the GMS, forest losses mainly in Cambodia and Thailand were also counteracted by forest gains during the study period mainly in China. Our estimated net gain of forest cover over the GMS is $2.5 \times 10^4 \text{ km}^2$ (0.96% of the region), which is closely consistent with the FAO-FRA and forest sector strategy 2020 (Leinenkugel et al., 2015).

The forest cover changes were closely associated with changes in C stocks, C density, and C sequestration: an increase in forest area corresponding to increases in C intensity and C sinks (comparing Figure 4 with Figures S5 and S6; Figure 1). Analysis of the effects of major forest cover transitions on C dynamics indicates that intact forests and new forests had higher contributions to C stocks and larger C sequestration than other forest land use types (Figure 3d–f). Forestry statistics at the national level showed that during the study period an increase in both C stocks and C sequestration in China due mainly to afforestation, and in Laos PDR and Myanmar due largely to

the large proportion of intact forests though there was a large area of deforestation. Our study also shows that the intact and newly planted forests substantially contributed to an increase in C sequestration (Table 1; Figure 3d–f). The degraded forest showed a strong positive impact on C loss (Figure 3d).

Political, social, and economic factors can influence forest conservation and transitions in conjunction with climate drivers. Market-driven intensification (Bruun et al., 2009, 2017; Davis et al., 2015; Grogan et al., 2019; Schmidt-Vogt et al., 2009; Zeng, Estes, et al., 2018) has led to accelerated forest loss and forest transformation in Cambodia, Thailand, and Laos PRD. National land-tenure policies and market pressures may have also increased local demands for new croplands in the GMS (Davis et al., 2015; Grogan et al., 2019). This expansion also stands in marked contrast to the widespread agricultural retreat and forest recovery that has been occurring in China where a series of government programs and rural-to-urban migration have returned farmland to forest on sloping highlands (Tong et al., 2020). The widespread and fast forest cover transitions in the GMS in this century have largely been ignored in both global assessments of land use and future projections, although which substantially influenced the roles tropical forests of this region play in the context of regional and global climate mitigation, biodiversity conservation, and global C cycling (Alkama & Cescatti, 2016; Baccini et al., 2017; Feng et al., 2021; Hansen et al., 2013, 2020; Matricardi et al., 2020; Saatchi et al., 2011). Our results not only should warrant the attention of policymakers, but also contribute to better understanding of the rapid and dramatic changes in forest cover transitions and associated C balance and to obtaining deeper insight into the causes of these changes. Our findings have potential implications for forest conservation, C sink service, and climate change mitigation in the GMS and other hotspots of tropical forests.

With regard to uncertainties in our analysis, to detect forest conversions at scales smaller than a Landsat pixel is beyond our ability

(Brinck et al., 2017) would lead to uncertainties. Our estimates represent absolute forest C losses, instead of net losses that incorporate biomass C gains that could not be calculated from available data with confidence (Feng et al., 2021). In addition, fragmentation and edge effects of forest losses causing additional long-term C losses on the landscape that we could not quantify (Zeng, Gower, & Wood, 2018). Comparison of our estimate of forest cover transitions during the period 1999–2019 over the GMS region with those four commonly used global land cover datasets (ESA-CCI, MCD12, VCF, and FRA) indicates more than 75% of matching pixels (Figures S7–S9). It is also noticed that uncertainties may stem from the errors in static datasets and scale mismatch between the benchmark C pools and remotely sensed forest C sequestration maps, however, the findings of this study provide up-to-date reference information on forest cover change and forest C uptake and a framework for the future extensive analysis of forest C dynamics and associated economic developments in the GMS. To reduce these uncertainties, future studies could integrate higher-resolution satellite and lidar datasets to map primary and secondary forests and related biomass C loss more accurately. More studies on above- and belowground C recovery associated with forest regrowth are also needed.

AUTHOR CONTRIBUTIONS

Baozhang Chen, Philippe Ciais and Shilong Piao designed the research; Alphonse Kayiranga and Mengyu Ge performed the analysis; Baozhang Chen, Alphonse Kayiranga, Philippe Ciais, Andy Black, and Zhenzhong Zeng led the writing and editing of the manuscript; Huifang Zhang, Mengyu Ge, Xiangming Xiao, and Wenping Yuan contributed to the interpretation of the results; and all authors contributed to data and to the text.

ACKNOWLEDGMENTS

This research was funded by National Key R&D Program of China (2018YFA0606001), National Natural Science Foundation of China (41771114), and Innovation Project of LREIS (No. KPI005).

CONFLICT OF INTEREST STATEMENT

The authors declare no competing interests.

DATA AVAILABILITY STATEMENT

MODIS land cover (MCD 12Q1) dataset can be downloaded from LP DAAC data pool at <https://e4ftl01.cr.usgs.gov/MOTA/MCD12Q1.006/>; GLC_FCS30 maps are available at <https://zenodo.org/record/3986872#.YJYz91ZfjiU>; ESA-CCL-LC-S2-prototype land cover map can be downloaded from <https://2018mexicolandcover10m.esa.int/>; ESA-CCI-LC-L4 maps are available at <http://maps.elie.ucl.ac.be/CCI/viewer/download.php>; Tsinghua global LC maps are available at <http://data.ess.tsinghua.edu.cn/> or http://data.ess.tsinghua.edu.cn/fromglc2015_v1.html; the global spatial temporal spectral Library (GSPECLib) LC validation points are available at http://data.ess.tsinghua.edu.cn/data/temp/GlobalLandCoverValidationSampleSet_v1.xlsx; the static benchmark maps of aboveground biomass and belowground biomass carbon pools were downloaded

from https://daac.ornl.gov/get_data/; soil organic carbon and forestry related tissues organic carbon data can be obtained from <http://www.fao.org/soils-portal/data-hub/soil-maps-and-databases/harmonized-world-soil-database-v12/en/>.

Code availability: The Google Earth Engine (GEE) scripts used in this study are derived from Landsat sensors and the data sources are available at: (1) Landsat ETM+: <https://code.earthengine.google.com/c8490ffccaf5cb0a16062585de66f48b>, and (2) Landsat 8 OLI: <https://code.earthengine.google.com/89e2d95da9d24e86415455bc2f2cd9c7>.

ORCID

Baozhang Chen  <https://orcid.org/0000-0001-8972-706X>

Xiangming Xiao  <https://orcid.org/0000-0003-0956-7428>

Zhenzhong Zeng  <https://orcid.org/0000-0001-6851-2756>

Shilong Piao  <https://orcid.org/0000-0001-8057-2292>

REFERENCES

- Alkama, R., & Cescatti, A. (2016). Biophysical climate impacts of recent changes in global forest cover. *Science*, 351(6273), 600–604.
- Baccini, A., Walker, W., Carvalho, L., Farina, M., Sulla-Menashe, D., & Houghton, R. A. (2017). Tropical forests are a net carbon source based on aboveground measurements of gain and loss. *Science*, 358(6360), 230–234.
- Bierbower, W. (2015). *InVEST 2.6. 0 users guide. The natural capital project*. The Natural Capital Project, Stanford University, University of Minnesota, The Nature Conservancy, and World Wildlife Fund. <https://doi.org/10.13140/RG.2.2.32693.78567>
- Bofana, J., Zhang, M., Nabil, M., Wu, B., Tian, F., Liu, W., Zeng, H., Zhang, N., Nangombe, S. S., & Cipriano, S. A. (2020). Comparison of different cropland classification methods under diversified agroecological conditions in the zambezi river basin. *Remote Sensing*, 12(13), 2096.
- Bonan, G. B. (2008). Forests and climate change: Forcings, feedbacks, and the climate benefits of forests. *Science*, 320(5882), 1444–1449.
- Brandt, M., Yue, Y., Wigneron, J. P., Tong, X., Tian, F., Jepsen, M. R., Xiao, X., Verger, A., Mialon, A., & Al-Yaari, A. (2018). Satellite-observed major greening and biomass increase in South China karst during recent decade. *Earth's Future*, 6(7), 1017–1028.
- Brienen, R. J., Phillips, O. L., Feldpausch, T. R., Gloor, E., Baker, T. R., Lloyd, J., Lopez-Gonzalez, G., Monteagudo-Mendoza, A., Malhi, Y., & Lewis, S. L. (2015). Long-term decline of the Amazon carbon sink. *Nature*, 519(7543), 344–348.
- Brinck, K., Fischer, R., Groeneveld, J., Lehmann, S., De Paula, M. D., Pütz, S., Sexton, J. O., Song, D., & Huth, A. (2017). High resolution analysis of tropical forest fragmentation and its impact on the global carbon cycle. *Nature Communications*, 8(1), 1–6.
- Bruun, T. B., de Neergaard, A., Burup, M. L., Hepp, C. M., Larsen, M. N., Abel, C., Aumtong, S., Magid, J., & Mertz, O. (2017). Intensification of upland agriculture in Thailand: Development or degradation? *Land Degradation & Development*, 28(1), 83–94.
- Bruun, T. B., De Neergaard, A., Lawrence, D., & Ziegler, A. D. (2009). Environmental consequences of the demise in swidden cultivation in Southeast Asia: Carbon storage and soil quality. *Human Ecology*, 37(3), 375–388.
- Chen, H., Zeng, Z., Wu, J., Peng, L., Lakshmi, V., Yang, H., & Liu, J. (2020). Large uncertainty on Forest area change in the early 21st century among widely used global land cover datasets. *Remote Sensing*, 12(21), 21. <https://doi.org/10.3390/rs12213502>
- Chu, X., Zhan, J., Li, Z., Zhang, F., & Qi, W. (2019). Assessment on forest carbon sequestration in the three-north shelterbelt program region, China. *Journal of Cleaner Production*, 215, 382–389.

- Costenbader, J., Broadhead, J., Yasmi, Y., & Durst, P. B. (2015). *Drivers affecting forest change in the Greater Mekong Subregion (GMS): An overview*. FAO.
- Davis, K. F., Yu, K., Rulli, M. C., Pichdara, L., & D'Odorico, P. (2015). Accelerated deforestation driven by large-scale land acquisitions in Cambodia. *Nature Geoscience*, *8*(10), 772–775.
- Delang, C. O., & Yuan, Z. (2016). *China's grain for green program*. Springer.
- Erb, K.-H., Kastner, T., Plutzer, C., Bais, A. L. S., Carvalhais, N., Fetzel, T., Gingrich, S., Haberl, H., Lauk, C., & Niedertscheider, M. (2018). Unexpectedly large impact of forest management and grazing on global vegetation biomass. *Nature*, *553*(7686), 73–76.
- Feng, Y., Ziegler, A. D., Elsen, P. R., Liu, Y., He, X., Spracklen, D. V., Holden, J., Jiang, X., Zheng, C., & Zeng, Z. (2021). Upward expansion and acceleration of forest clearance in the mountains of Southeast Asia. *Nature Sustainability*, *4*, 892–899. <https://doi.org/10.1038/s41893-021-00738-y>
- Foley, J. A., DeFries, R., Asner, G. P., Barford, C., Bonan, G., Carpenter, S. R., Chapin, F. S., Coe, M. T., Daily, G. C., & Gibbs, H. K. (2005). Global consequences of land use. *Science*, *309*(5734), 570–574.
- Fortin, J. A., Cardille, J. A., & Perez, E. (2020). Multi-sensor detection of forest-cover change across 45 years in Mato Grosso, Brazil. *Remote Sensing of Environment*, *238*, 111266.
- Gardner, T. A., Barlow, J., Chazdon, R., Ewers, R. M., Harvey, C. A., Peres, C. A., & Sodhi, N. S. (2009). Prospects for tropical forest biodiversity in a human-modified world. *Ecology Letters*, *12*, 561–582. <https://doi.org/10.1111/j.1461-0248.2009.01294.x>
- Gong, P., Li, X., & Zhang, W. (2019). 40-Year (1978–2017) human settlement changes in China reflected by impervious surfaces from satellite remote sensing. *Science Bulletin*, *64*(11), 756–763.
- Gritten, D., Lewis, S. R., Breukink, G., Mo, K., Thuy, D. T. T., & Delattre, E. (2019). Assessing forest governance in the countries of the Greater Mekong Subregion. *Forests*, *10*(1), 47.
- Grogan, K., Pflugmacher, D., Hostert, P., Mertz, O., & Fensholt, R. (2019). Unravelling the link between global rubber price and tropical deforestation in Cambodia. *Nature Plants*, *5*(1), 47–53.
- Hansen, A. J., Burns, P., Ervin, J., Goetz, S. J., Hansen, M., Venter, O., Watson, J. E., Jantz, P. A., Virnig, A. L., & Barnett, K. (2020). A policy-driven framework for conserving the best of Earth's remaining moist tropical forests. *Nature Ecology & Evolution*, *4*(10), 1377–1384.
- Hansen, M. C., & DeFries, R. S. (2004). Detecting long-term global Forest change using continuous fields of tree-cover maps from 8-km advanced very high resolution radiometer (AVHRR) data for the years 1982–99. *Ecosystems*, *7*(7), 695–716. <https://doi.org/10.1007/s10021-004-0243-3>
- Hansen, M. C., Potapov, P. V., Moore, R., Hancher, M., Turubanova, S. A., Tyukavina, A., Thau, D., Stehman, S., Goetz, S. J., & Loveland, T. R. (2013). High-resolution global maps of 21st-century forest cover change. *Science*, *342*(6160), 850–853.
- Huang, B., Huang, J., Pontius, R. G., Jr., & Tu, Z. (2018). Comparison of intensity analysis and the land use dynamic degrees to measure land changes outside versus inside the coastal zone of Longhai, China. *Ecological Indicators*, *89*, 336–347.
- Hui, D., Deng, Q., Tian, H., & Luo, Y. (2017). Climate change and carbon sequestration in forest ecosystems. In W. Y. Chen, T. Suzuki, & M. Lackner (Eds.), *Handbook of climate change mitigation and adaptation* (pp. 555–594). Springer.
- Kayiranga, A., Kurban, A., Nahayo, L., & Ndayisaba, F. (2018). Assessing Forest cover changes in volcanoes parks region of east-Central Africa using Landsat imagery. *Journal of Environment Protection and Sustainable Development*, *4*(2), 16–25.
- Kayiranga, A., Kurban, A., Ndayisaba, F., Nahayo, L., Karamage, F., Ablekim, A., Li, H., & Ilniyaz, O. (2016). Monitoring forest cover change and fragmentation using remote sensing and landscape metrics in Nyungwe-Kibira park. *Journal of Geoscience and Environment Protection*, *4*(11), 13–33.
- Keenan, T., Baker, I., Barr, A., Ciais, P., Davis, K., Dietze, M., Dragoni, D., Gough, C. M., Grant, R., & Hollinger, D. (2012). Terrestrial biosphere model performance for inter-annual variability of land-atmosphere CO₂ exchange. *Global Change Biology*, *18*(6), 1971–1987.
- Kwon, Y., & Larsen, C. P. (2013). Effects of forest type and environmental factors on forest carbon use efficiency assessed using MODIS and FIA data across the eastern USA. *International Journal of Remote Sensing*, *34*(23), 8425–8448.
- Leinenkugel, P., Wolters, M. L., Oppelt, N., & Kuenzer, C. (2015). Tree cover and forest cover dynamics in the Mekong Basin from 2001 to 2011. *Remote Sensing of Environment*, *158*, 376–392.
- Li, C., Wang, J., Wang, L., Hu, L., & Gong, P. (2014). Comparison of classification algorithms and training sample sizes in urban land classification with Landsat thematic mapper imagery. *Remote Sensing*, *6*(2), 964–983.
- Liang, Y., Liu, L., & Huang, J. (2017). Integrating the SD-CLUE-S and InVEST models into assessment of oasis carbon storage in north-western China. *PLoS One*, *12*(2), e0172494.
- Lin, X., Xu, M., Cao, C., Singh, P. R., Chen, W., & Ju, H. (2018). Land-use/land-cover change and their influence on the ecosystem in Chengdu City, China during the period of 1992–2018. *Sustainability*, *10*(10), 3580.
- Liu, C., Li, W., Zhu, G., Zhou, H., Yan, H., & Xue, P. (2020). Land use/land cover changes and their driving factors in the northeastern Tibetan plateau based on geographical detectors and Google Earth Engine: A case study in Gannan prefecture. *Remote Sensing*, *12*(19), 3139.
- Liu, L., Xiao, X., Qin, Y., Wang, J., Xu, X., Hu, Y., & Qiao, Z. (2020). Mapping cropping intensity in China using time series Landsat and Sentinel-2 images and Google Earth Engine. *Remote Sensing of Environment*, *239*, 111624.
- MacDicken, K. G. (2015). Global forest resources assessment 2015: What, Why and How? *Forest Ecology and Management*, *352*, 3–8. <https://doi.org/10.1016/j.foreco.2015.02.006>
- Matricardi, E. A. T., Skole, D. L., Costa, O. B., Pedlowski, M. A., Samek, J. H., & Miguel, E. P. (2020). Long-term forest degradation surpasses deforestation in the Brazilian Amazon. *Science*, *369*(6509), 1378–1382.
- Moore, R., & Hansen, M. (2011). *Google Earth Engine: A new cloud-computing platform for global-scale earth observation data and analysis*. In Proceedings of the AGU Fall Meeting (Abstract id. IN43C-02). <https://ui.adsabs.harvard.edu/abs/2011AGUFMIN43C.02M/abstract>
- Münch, Z., Gibson, L., & Palmer, A. (2019). Monitoring effects of land cover change on biophysical drivers in rangelands using albedo. *Land*, *8*(2), 33.
- Namkhan, M., Gale, G. A., Savini, T., & Tantipisanuh, N. (2021). Loss and vulnerability of lowland forests in mainland Southeast Asia. *Conservation Biology*, *35*(1), 206–215.
- Nitze, I., Schulthess, U., & Asche, H. (2012). *Comparison of machine learning algorithms random forest, artificial neural network and support vector machine to maximum likelihood for supervised crop type classification*. Proc. of the 4th GEOBIA, 35.
- Pungkul, S., Suraswasdi, C., & Phonekeo, V. (2014). Implementation of forest cover and carbon mapping in the Greater Mekong Subregion and Malaysia project—a case study of Thailand. *IOP Conference Series: Earth and Environmental Science*, *18*(1), 012141.
- Qin, Y., Xiao, X., Dong, J., Zhang, Y., Wu, X., Shimabukuro, Y., Arai, E., Biradar, C., Wang, J., & Zou, Z. (2019). Improved estimates of forest cover and loss in the Brazilian Amazon in 2000–2017. *Nature Sustainability*, *2*(8), 764–772.
- Saatchi, S. S., Harris, N. L., Brown, S., Lefsky, M., Mitchard, E. T., Salas, W., Zutta, B. R., Buermann, W., Lewis, S. L., & Hagen, S. (2011). Benchmark map of forest carbon stocks in tropical regions across three continents. *Proceedings of the National Academy of Sciences of the United States of America*, *108*(24), 9899–9904.

- Schmidt-Vogt, D., Leisz, S. J., Mertz, O., Heinemann, A., Thiha, T., Messerli, P., Epprecht, M., Van Cu, P., Chi, V. K., & Hardiono, M. (2009). An assessment of trends in the extent of swidden in Southeast Asia. *Human Ecology*, 37(3), 269.
- Keenan, R. J., Reams, G. A., Achard, F., de Freitas, J. V., Grainger, A., & Lindquist, E. (2015). *Dynamics of global forest area: Results from the FAO Global Forest Resources Assessment 2015*. ScienceDirect. <https://www.sciencedirect.com/science/article/pii/S0378112715003400>
- Song, X.-P., Hansen, M. C., Stehman, S. V., Potapov, P. V., Tyukavina, A., Vermote, E. F., & Townshend, J. R. (2018). Global land change from 1982 to 2016. *Nature*, 560(7720), 639–643.
- Tang, X., Woodcock, C. E., Olofsson, P., & Hutya, L. R. (2021). Spatiotemporal assessment of land use/land cover change and associated carbon emissions and uptake in the Mekong River basin. *Remote Sensing of Environment*, 256, 112336. <https://doi.org/10.1016/j.rse.2021.112336>
- Thanh Noi, P., & Kappas, M. (2018). Comparison of random forest, k-nearest neighbor, and support vector machine classifiers for land cover classification using Sentinel-2 imagery. *Sensors*, 18(1), 18.
- Tong, X., Brandt, M., Yue, Y., Ciais, P., Jepsen, M. R., Penuelas, J., Wigneron, J.-P., Xiao, X., Song, X.-P., & Horion, S. (2020). Forest management in southern China generates short term extensive carbon sequestration. *Nature Communications*, 11(1), 1–10.
- Tong, X., Brandt, M., Yue, Y., Horion, S., Wang, K., De Keersmaecker, W., Tian, F., Schurgers, G., Xiao, X., & Luo, Y. (2018). Increased vegetation growth and carbon stock in China karst via ecological engineering. *Nature Sustainability*, 1(1), 44–50.
- Yasmi, Y., Durst, P., Haq, R. U., & Broadhead, J. (2017). *Forest change in the Greater Mekong Subregion (gms) an overview of negative and positive drivers*. The Food and Agriculture Organization of the United Nations (FAO).
- Yin, Y., Bloom, A. A., Worden, J., Saatchi, S., Yang, Y., Williams, M., Liu, J., Jiang, Z., Worden, H., & Bowman, K. (2020). Fire decline in dry tropical ecosystems enhances decadal land carbon sink. *Nature Communications*, 11(1), 1–7.
- Zeng, Z., Estes, L., Ziegler, A. D., Chen, A., Searchinger, T., Hua, F., Guan, K., Jintrawet, A., & Wood, E. F. (2018). Highland cropland expansion and forest loss in Southeast Asia in the twenty-first century. *Nature Geoscience*, 11(8), 556–562.
- Zeng, Z., Gower, D. B., & Wood, E. F. (2018). Accelerating forest loss in southeast Asian massif in the 21st century: A case study in Nan Province, Thailand. *Global Change Biology*, 24(10), 4682–4695.
- Zheng, H., Du, P., Chen, J., Xia, J., Li, E., Xu, Z., Li, X., & Yokoya, N. (2017). Performance evaluation of downscaling Sentinel-2 imagery for land use and land cover classification by spectral-spatial features. *Remote Sensing*, 9(12), 1274.

SUPPORTING INFORMATION

Additional supporting information can be found online in the Supporting Information section at the end of this article.

How to cite this article: Chen, B., Kayiranga, A., Ge, M., Ciais, P., Zhang, H., Black, A., Xiao, X., Yuan, W., Zeng, Z., & Piao, S. (2023). Anthropogenic activities dominated tropical forest carbon balance in two contrary ways over the Greater Mekong Subregion in the 21st century. *Global Change Biology*, 00, 1–12. <https://doi.org/10.1111/gcb.16688>